

Exploring the structural, electronic and magnetic properties of cation ordered 3d-5d double perovskite $\text{Bi}_2\text{FeReO}_6$ and $\text{Bi}_2\text{FeIrO}_6$ thin-films from first-principles

Paresh C. Rout⁽¹⁾ and Varadharajan Srinivasan^(1,2)

(1) Department of Physics, Indian Institute of Science Education and Research Bhopal, Bhopal 462 066, India and

(2) Department of Chemistry, Indian Institute of Science Education and Research Bhopal, Bhopal 462 066, India

We report a first-principles study of Bi-based 3d-5d ordered double perovskite oxides ($\text{A}_2\text{BB}'\text{O}_6$) with a 3d atom (Fe) at the B-site and 5d atoms (Re, Ir) at the B'-site while keeping highly polarizable ions (Bi^{3+}) at the A-site. We find that, under coherent heteroepitaxy, $\text{Bi}_2\text{FeReO}_6$ exhibits a strain-driven anti-ferromagnetic insulator to ferrimagnetic semi-metal transition, while $\text{Bi}_2\text{FeIrO}_6$ shows correlation driven ferromagnetic insulator to ferrimagnetic half-metal transition with calculated magnetic moments of $5 \mu_B/\text{f.u.}$ and $3 \mu_B/\text{f.u.}$, respectively. These properties along with the low band gaps in the insulating phases make the compounds appealing for spintronics applications. Furthermore, in $\text{Bi}_2\text{FeIrO}_6$, the conduction and valence states are localized on different transition metal sublattices implying more efficient electron-hole separation upon photoexcitation, a desirable feature for photovoltaic applications.

PACS numbers: 77.55.Nv, 75.50.Gg, 75.50.-i, 75.10.-b, 75.25.-j, 75.30.-m, 75.80.+q

INTRODUCTION

Transition metal (TM) double-perovskites (DP) ($\text{A}_2\text{BB}'\text{O}_6$) have gained enormous attention recently due to their fascinating properties in the areas of magnetism, ferroelectrics, spintronics and multiferroics [1] and long served as a platform for device applications. Particularly, multiferroic materials are quite promising due to their multipurpose technological implications [2, 3]. These materials are characterized by coexistence of ferroic orders such as ferroelectricity, ferromagnetism and/or ferroelasticity along with a coupling of at least two of these orders which can, in turn, lead to magnetoelectric, magnetoelastic effects, etc. A prominent example of DP multiferroic is $\text{Bi}_2\text{FeCrO}_6$ (BFCO), which was designed from the AFM parent multiferroic compound BiFeO_3 (BFO) by replacing half the Fe ions by Cr with an aim to increase the magnetic moment through ferrimagnetic interaction of B and B' sites while retaining ferroelectricity and magneto-electric coupling intact [4]. Due to AFM ordering, the parent compound BFO shows ~ 0 magnetic moment, however, BFCO was predicted to show a magnetic moment of $2 \mu_B$ per formula unit (f.u.) in its bulk form with a G-type AFM ordering.

In practice, multiferroics can be prepared as high quality epitaxial thin films on oxide substrates. The epitaxial strain (ES), which can be introduced by varying lattice mismatch between the thin-film and substrate, has the tendency to control the material properties and to stabilize other metastable magnetic structures [5–9]. The potential of multiferroic materials towards photovoltaic (PV) and photocatalytic (PC) application is currently being explored. The narrow band gap, which arises due to electron-electron interaction governing the magnetic ordering, makes multiferroics special candidates for PV application over the general perovskite materials [10]. Among multiferroics, BFO was considered to show appreciable PV effect due to the presence of a direct band gap, a fact latter corroborated by Chui *et al.* [11]. However, the power conversion efficiency (PCE) of BFO based thin film devices is still very low for practical application. Lowering the band gap of

these oxides without affecting their FE properties is a promising conceptual route to obtain solar energy conversion devices with higher PCE. Recently, it was shown that the epitaxial multiferroic ordered BFCO thin-films possess a power conversion efficiency of 6.5% under the illumination of red light laser [12] and 8.1% under AM1.5G illumination [13]. In both the works, it was pointed out that the Fe and Cr cation order and the narrow band gap play a crucial role in the PV performance of BFCO thin films. Kim *et al.* [14] recently attributed the excellent performance of BFCO to the spatial separation of the photoexcited electron and hole states onto the Fe and Cr sites, respectively, with the extent of separation increasing with the disorder at the B-site.

Recently, we have shown that epitaxially grown (001) BFCO thin-films are unstable to anti-site defects and prefer a C-type AFM (C-AFM) ordered ground state [15], both features leading to loss of magnetization [16–18]. The anti-site defects (disordering) occur basically due to the similarity of charge and ionic radii of Fe^{3+} and Cr^{3+} ions. We have also recently shown that by manipulating both ES and aliovalent A-site doping in BFCO thin films [19], one can not only mitigate the issues like cation disorder and low magnetism but also significantly reduce the band gap, a desirable feature for PV applications. An alternative approach to suppress B-site disorder and encode functionality in Bi-based DPs is to form 3d-5d oxides [20]. Doping with 5d TM ions can not only improve magnetisation but also prevent the formation of antisite defects like BFCO thin-films due to their larger sizes compared to the 3d ions. Apart from this, the mixture of 3d-5d ions would likely improve the transition temperature as seen in case of Ca, Sr-based systems, due to the induced magnetic moment at the nonmagnetic sites [21, 22].

In this work, we investigate the strain-dependent magnetic and electronic properties of two new double-perovskite 3d-5d systems: $\text{Bi}_2\text{FeReO}_6$ (BFRO) and $\text{Bi}_2\text{FeIrO}_6$ (BFIO) from first-principles DFT simulations. BFO was chosen as a starting point for the doping with 5d ions given its robust ferroelectric nature. We chose Fe atom as the 3d ion in the B-site as

it usually occurs in high-spin 3+ oxidation state, which could lead to large magnetic moment in DPs, stronger magnetic interactions and hence larger transition temperatures.

Our calculations predict an anti-polar $P2_1/n$ -like structure for both compounds if grown on cubic substrates. We find that a C-type AFM ordering is favored for BFRO, while BFIO becomes a ferromagnetic insulator through out the ES region. In

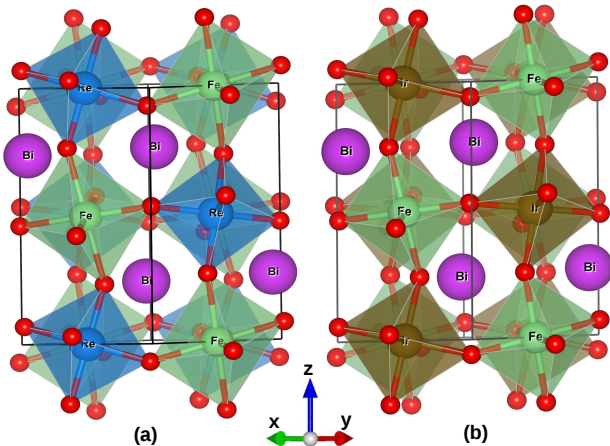


FIG. 1. Strained bulk tetragonal supercell used for modeling the thin-films (001) for calculations. (a) The tetragonal supercell of $\text{Bi}_2\text{FeReO}_6$ with $a^- a^- c^+$ oxygen octahedra tilt pattern, (b) Represents, the tetragonal supercell of $\text{Bi}_2\text{FeIrO}_6$ with same octahedra orientation as indicated in (a). Both the structure has $P2_1/n$ symmetry.

BFRO thin-films, we show that at higher compressive strain, there is a C to G-AFM ($1\mu_B/f.u.$) transition accompanied by monoclinic to monoclinic structural transition due to octahedral reorientation. However, in BFIO thin-films, we find a correlation driven metal-to-insulator transition under ES. We find that the 3d and 5d cations adopt high spin 2+ and 4+ oxidation state (denoted below as (2+,4+)), respectively, in case of BFRO thin films. In BFIO, however, there is a competition between (2+,4+) and (3+,3+) states affected by onsite correlation at the low-spin Ir sites. We predict that correlation effects along with the stability of the 3+ oxidation state on the high-spin Fe sites will lead to the stabilisation of the (3+,3+) state in BFIO, with a magnetic moment of $5\mu_B/f.u.$, under all ES. Furthermore, BFRO is predicted to be an AFM insulator under ES, whereas the Ir-based DP is a ferromagnetic insulator. Ferromagnetic insulators (FM-I) are rare and very promising for their spintronics and PV applicability [5, 23]. So far, most of the synthesized 3d-5d DP materials are half-metallic in nature. However, $\text{Bi}_2\text{FeIrO}_6$ is a promising material as it exhibits both ferromagnetism and insulating properties simultaneously. Considering the presence of 5d elements, we included SOC in our calculation but found that SOC does not have a significant effect on the magnetic properties while it has a small impact on the electronic properties, particularly resulting in a slight band gap reduction. We show that the correlation effect on 5d site plays a very crucial in opening

the band gap and magnetic phase transition, which was completely ignored in the previous study [24]. Presence of very narrow band gap ~ 1.1 eV in both the compounds (considering correlation effect on both 3d-5d ions) makes them suitable candidates for PV applications.

METHOD OF CALCULATION

Our calculations employed a spin-polarized GGA+ U [25–27] approach using the revised version Perdew-Burke-Ernzerhof (PBE) [28, 29] for solids, PBEsol [30] as exchange-correlation functional within the framework of the Quantum-ESPRESSO code [31]. Ionic cores were modeled by ultrasoft pseudopotentials keeping the 4f electrons of 5d transition metals and Bi atoms as part of the core. Plane-wave cut-off energy of 85 Ry was used for representing wavefunctions, and 700 Ry for the augmentation charge. The Hubbard U parameter can be calculated *ab initio* using the linear response formalism [26, 27]. We found the U values to be 6.4 eV (Fe) and 3.6 eV (Re) in BFRO system, whereas in BFIO case, the U values were 6.38 (Fe) and 5.18 (Ir). We used a $10 \times 10 \times 8$ Monkhorst-Pack k-point mesh for Brillouin zone integration. For the density of states (DOS) calculations, a denser Monkhorst-Pack k-point grid of $16 \times 16 \times 16$ was employed. All the structures were relaxed until the Hellmann-Feynmann forces are less than 0.26 meV/Å.

For both the compounds, we have constructed 20-atom $\sqrt{2} \times \sqrt{2} \times 2$ tetragonal supercells (shown in Figure 1), starting from a simple cubic double-perovskite structure, to allow for appropriate magnetic ordering of ions along (111) direction. The structures were chosen to conform to $P2_1/n$ (antipolar) and $R3$ (polar) space groups, respectively, given their compatibility with cubic substrates [16, 18]. These essentially differ by the sense and relative magnitudes of oxygen octahedral rotations as indicated by the Glazer notations $a^- a^- c^+$ and $a^- a^- a^-$, respectively [32, 33]. Using the substrate SrTiO_3 pseudo-cubic lattice parameter $a_{cub} = 3.90\text{Å}$ [34] as a reference, we generated structures mimicking the epitaxially strained films by varying the in-plane lattice parameters over a range of realistic substrate strains corresponding to (001) epitaxial growth. The in-plane lattice parameters of supercell are set to $\bar{a} = \bar{b} = \sqrt{2} \times a_{cub}$ while the c parameters have been relaxed for each in-plane strain. The ES can be defined as

$$\epsilon = (\bar{a} - \bar{a}_{ref}) / \bar{a}_{ref} \quad (1)$$

where \bar{a}_{ref} is the unstrained lattice parameter. The selection of Re and Ir structures is based on the adapted tolerance factor t of the double-perovskites [35]. The tolerance factor for DPs $\text{A}_2\text{BB}'\text{O}_6$, can be written as:

$$t = \frac{r_A + r_O}{\sqrt{2} \times \left(\frac{r_B}{2} + \frac{r_{B'}}{2} + r_O \right)} \quad (2)$$

where r_A , r_B and $r_{B'}$ are the ionic radii of the respective ions and r_O is the ionic radius of oxygen. It is known that, for

double-perovskite family, if $t < 0.97$ the compound becomes either monoclinic ($P2_1/n$) or orthorhombic [36]. In case of $\text{Bi}_2\text{FeReO}_6$, the calculated average tolerance factor is 0.93 while for $\text{Bi}_2\text{FeIrO}_6$, it is 0.95. Hence, both structures are expected to take perovskite form.

RESULTS AND DISCUSSIONS

Strain-dependence ground-state structure of $\text{Bi}_2\text{FeReO}_6$

We first investigated the effect of ES on the ground-state structure of BFRO compound. We considered three types of AFM (A, C, G-type) and the FM orders for the calculations [15]. We have considered the two lowest energy phases $P2_1/n$ and $R3$ phase, which were also previously found to be stable for similar systems under various strains [24]. The ES is introduced in thin-film by constraining the two in-plane lattice vectors to be equal in length and enforce the angle between them to be 90° . We first obtained the optimized geometries

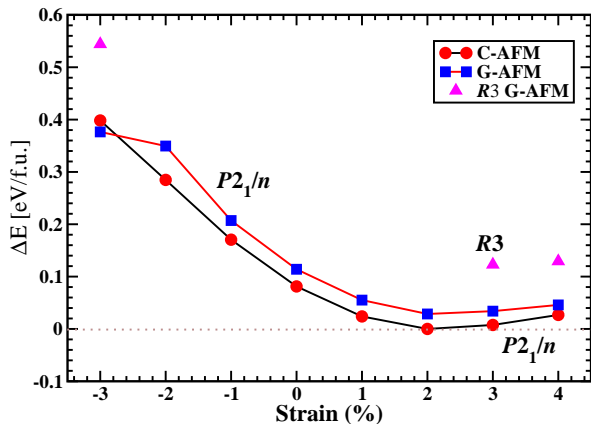


FIG. 2. Energy vs strain for the two lowest energy magnetic ordering of $P2_1/n$ structure. The energy of $R3$ structure indicated by magenta upper triangle are plotted at at higher compressive and tensile strain region. All the energies are positioned with respect to the lowest energy of C-AFM ordering in $P2_1/n$ symmetry. A crossover between G-AFM and C-AFM ordering occurs at -2.7% strain.

tries in the $P2_1/n$ and $R3$ phases for different magnetic orderings at all the considered ES. The minimum energy structure at each strain was obtained by allowing the length and angle of out-of-plane lattice parameter to relax simultaneously along with the ionic positions. Figure 2 depicts the energy (relative to the global minimum structure, i.e. $P2_1/n$ at 2% strain) of the lowest lying states as a function of ES. From Figure 2, it is clear that the ferroelectric phase ($R3$) is not favorable under the considered epitaxial strains. We find that C-AFM of $P2_1/n$ phase is the most stable structure over the broad range of strain leading to zero total magnetic moment due to exact cancellation of the spin magnetic moment. Most interestingly, a magnetic ordering transition (from C-AFM to G-AFM) is seen at -2.7% , which suggests that a net magnetic moment can

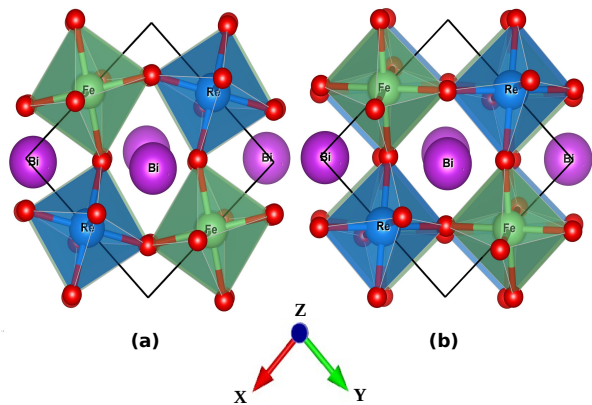


FIG. 3. (a) Out-of-plane (top) view of G-AFM $\text{Bi}_2\text{FeReO}_6$ structure, (b) Out-of-plane (top) view of C-AFM $\text{Bi}_2\text{FeReO}_6$ structures at -2.7% strain.

also be achieved in $\text{Bi}_2\text{FeReO}_6$ thin-films through compressive strain. We ascribe the magnetic phase transition to the oxygen octahedra reorientation induced monoclinic to monoclinic structural transition. The structures of both C and G-AFM BFRO are shown in Figure 3 and the corresponding structural information for both the magnetic ordered structure at -2.7% strain are provided in Table I. The monoclinic angle

TABLE I. Structural information for both C-AFM and G-AFM magnetic ordering at -2.7% strain.

Type	a (Å)	b (Å)	c (Å)	α ($^\circ$)	β ($^\circ$)	γ ($^\circ$)
C-AFM	5.364	5.364	8.652	90.00	90.28	90.00
G-AFM	5.364	5.364	9.094	90.00	84.75	90.00

(angle between a and c lattice parameters) changes from being obtuse in the C-AFM to be acute in the G-AFM structure. This transformation results from a sudden oxygen octahedra reorientation at -2.7% strain (see Figure 3). So, beyond -2.7% strain, magnetic ground-state for BFRO can be achieved with a magnetic moment of $1\mu_B/\text{f.u.}$. The polar $R3$ phase, however, remains higher in energy in this strain region. One unusual finding in case of BFRO thin-film is the oxygen octahedral distortion around the Fe atom. It was observed that the Fe atom undergoes a Jahn-Teller-like distortion, leading to three different types of Fe-O bond length whereas the Re atom remains undisturbed. The three unequal bonds at reference (0% strain) are axial Fe-O_{ax} long bond (2.28 Å), equatorial Fe-O_{eq} medium bond (2.14 Å) and apical Fe-O_{ap} short bond (2.05 Å). This octahedral distortion pattern is also seen in other strain regions.

Electronic and magnetic properties of $\text{Bi}_2\text{FeReO}_6$

In this section, we analyze the electronic structure of $\text{Bi}_2\text{FeReO}_6$ thin-films in the antipolar $P2_1/n$ structure. We

also briefly discuss about the magnetic properties of the corresponding structure.

We find that the BFRO structure prefers to adopt C-AFM ordering, where the spins on Fe ($3d$) and Re ($5d$) transition metal ions anti-aligned in the plane of epitaxy (in-plane) but align parallelly perpendicular to this plane (out-of-plane). However, the structure undergoes a magnetic phase transition beyond -2.7% strain leading to a G-AFM ordered phase where the spins are anti-aligned both in-plane and out-of-plane. The total density of states (DOS) and the contributions to it from the d and p states of Fe (Re) and O, respectively, for both the spin channels, calculated within GGA+ U (only on Fe) at reference strain (0%) are shown in Figure 4(a). In BFRO, Re prefers $4+$ oxidation state (high spin) and Fe prefers to stay in high spin $2+$ oxidation state. The thick black line represents the total DOS for both the spin channels (spin up and down). The up and down channels contribute equally to the DOS indicating an AFM ground state. The orange solid line represents the local density of states (LDOS) for Fe ($3d$) orbitals and the solid blue lines LDOS for $5d$ (Re) states. The LDOS which arise from oxygen p orbitals, denoted by magenta color, contribute predominantly to the total density of states (see Figure 4(a)). The structure is insulating, with a small gap of 0.4 eV in the GGA+ U calculations. However, this gap is significantly enhanced up to 1.2 eV after incorporating onsite Coulomb repulsion $U = 3.6$ eV on Re-sites as shown in Figure 4(b). This suggests that the correlation effects arising from Re atoms would be important in this system. The band near the Fermi energy arises predominantly from Re $5d$ (t_{2g}) states with strong oxygen $2p$ orbital hybridization. The bands just above the Fermi level have a predominantly Re $5d$ (e_g) character in both spin channels. The Fe t_{2g} bands lie between -8.5 to -5 eV for both the spin channels while the e_g bands extend from -5 to about -1.8 eV below the Fermi energy. There are two in-plane and one out-of-plane Fe-O-Re angles measuring 141° , 149° and 148° , respectively. The two in-plane angles are different due to oxygen octahedral distortion around the Fe atom. With these angular orientations, the magnetic moments on Fe and Re are coupled through anti-ferromagnetic superexchange mechanism [37–39] along the in-plane direction and coupled ferromagnetically along out-of-plane.

Similarly, the DOS for G-AFM at -2.7% strain is also shown in Figure 5. Here, the correlation effect on both Fe and Re-sites are taken into account for the DOS calculations. Unlike the C-AFM phase, in this case, neither the total DOS nor the LDOS are identical in both the spin channels. The difference in the DOS indicates the ferrimagnetic (FiM) nature of the compound. The t_{2g} bands of Fe are sharply localized within -8.5 to -6.0 eV energy window, while the t_{2g} states of Re-sites are localized in the minority spin channel immediately below the Fermi energy. Interestingly, the valence and conduction band edges correspond to different spin channels and there is no gap in between. Hence, there is an insulator (C-AFM) to semi-metal (G-AFM) transition at -2.7% strain. The half-metallic (or semi-metallic) state (see Figure 5) results de-

spite using U on both the TM sites, making it less likely to be an artifact of the DFT method employed. This is indeed one of our important findings in this compound under ES.

Strain-dependence ground-state structure of $\text{Bi}_2\text{FeIrO}_6$

In this section, we have studied the influence of ES on $\text{Bi}_2\text{FeIrO}_6$ thin-films. The ionic positions and the corresponding c -axis at each strain are optimized by using GGA+ U (used U only on Fe) approach in $P2_1/n$ symmetry. We also studied the effect of U on Ir ($5d$) sites as it plays a very crucial role in predicting the electronic properties as seen in the previous section. The optimized energies are plotted against the ES as shown in Figure 6 which shows the lowest energy magnetic states with large magnetic moments due to the existence of different oxidation numbers in the TM ions. As can be seen in Figure 6(a), the G-AFM emerged as the lowest energy state throughout the epitaxial strain. The FiM ground-state (solid black pointed circle line) possesses a $2+$ (Fe) and $4+$ (Ir) oxidation state which contributes to a net magnetic moment of $3 \mu_B/\text{f.u.}$, while the solid square pointed line represents the higher energy ferromagnetic structure with $3+$ (Fe) and $3+$ (Ir) oxidation states. In both the cases, the Fe-site assumes a high-spin configuration while Ir prefers low-spin. Note that the energy vs strain (Figure 6(a)) was obtained by using the GGA+ U approach, where the on-site Coulomb repulsion only included for Fe-site. However, keeping the necessity of U values on $5d$ -sites in mind [40], when we added U (5.18 eV) on Ir sites, we observed a sudden change in the ground state. Moreover, adding U on Ir sites the FiM ($2+$, $4+$) state no longer remains as the lowest energy state. Instead, the ferromagnetic ($3+$, $3+$) state get stabilized under strain (see Figure). The FiM ($2+$, $4+$) state denoted by solid black line is shifted up in energy while the energy of the ($3+$, $3+$) state, represented by the solid red line, is brought down significantly as compared to Figure 6(a). The ferromagnetic ground-state leads to a total magnetic moment of $5 \mu_B/\text{f.u.}$, which comes predominantly from the Fe sites, while the Ir ion undergoes a low spin d^6 configuration. In the Bi-based $3d$ - $5d$ compounds, this is a first observation of a $3+$ ($3d$), $3+$ ($5d$) states. In this compound, the magnetic moments of Fe atoms are aligned ferromagnetically and the induced moments on Ir sites are almost zero due to the low spin configuration as a result of which the total system becomes ferromagnetic.

The high U value calculated for Ir is contrary to the usual expectation of lowered correlations in the more diffuse $5d$ levels. Hence, we tested the robustness of the ($3+$, $3+$) state by scanning the U (Ir) keeping the U (Fe) fixed at 6.38 eV. The results are summarized in Figure 7. We observed that, even at a lower U value of 1.0 eV, the system already undergoes a transition from ferrimagnetic (Fe^{2+} , Ir^{4+}) to ferromagnetic (Fe^{3+} , Ir^{3+}) state. The energy of ferromagnetic states lowers further as we increase U (Ir) towards our calculated value ($U = 5.18$ eV). This result indicates that, correlation effects at Ir play an important role in BFIO making the FiM to FM tran-

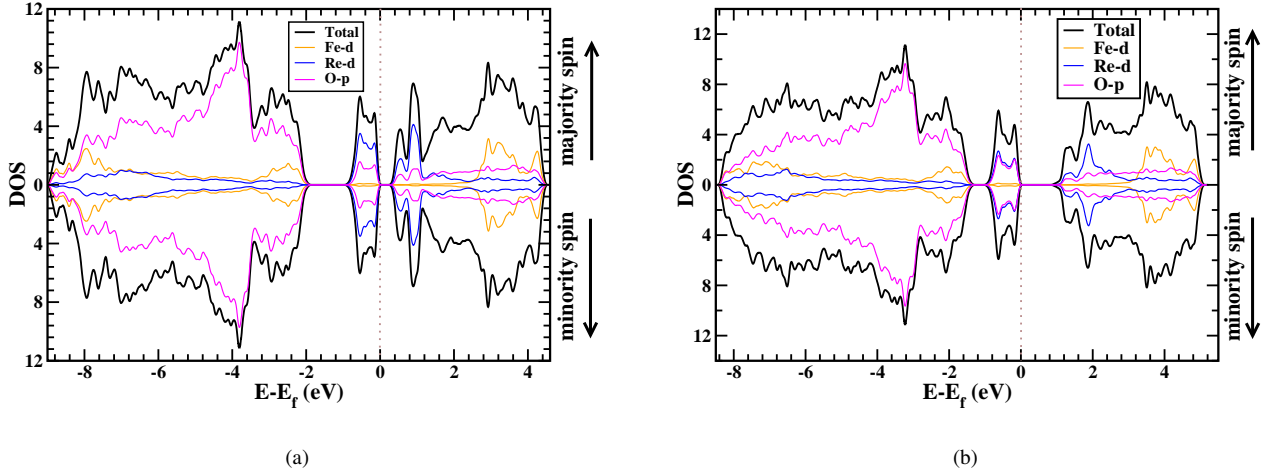


FIG. 4. (a) Density of states (DOS) plot of ground-state $\text{Bi}_2\text{FeReO}_6$ structure by adding U only on Fe-site. The solid black line, total DOS for both majority and minority spin channels; orange line, Fe- d orbitals; blue solid lines Re- d orbitals and solid magenta for O- p states. The local magnetic moments on Fe and Re are exactly antialigned. (b) Depicts DOS for $\text{Bi}_2\text{FeReO}_6$ by adding on-site Coulomb repulsion U on both Fe and Re-site. The color code has the same meaning as mentioned in (a). The band gap enhanced up to 1.2 eV, making the system into a robust insulator.

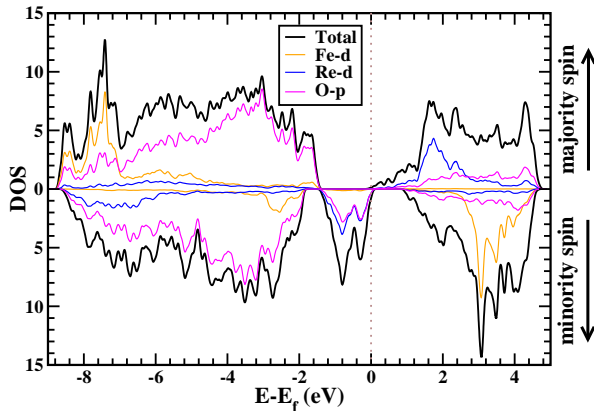


FIG. 5. The density of states (DOS) of G-type AFM $\text{Bi}_2\text{FeReO}_6$ at -2.7% strain calculated using GGA+ U method with $U_{\text{eff}}=6.4, 3.6$ eV for Fe and Re, respectively. The dashed vertical zero line is set to the Fermi energy. The local magnetic moments on Fe and Re are antialigned with unequal magnitude leading to a net magnetic moment on the system. The solid black line, total DOS; orange solid line, Fe- d states; blue line, Re- d states and solid magenta line, O- p states.

sition a correlation driven one. We have also scanned the U values for Fe-sites by fixing the U values of Ir-sites to zero. interestingly the same phase transition was observed at $U = 5.8$ eV, below which the system prefers to stay in the FM state while above it, the FiM state gets stabilized.

Electronic and magnetic properties of $\text{Bi}_2\text{FeIrO}_6$

In this section, we analyze the magnetic and electronic properties of DP $\text{Bi}_2\text{FeIrO}_6$ thin-films in detail. The DOS of both the possible (FM and FiM) phases are studied and are shown in Figure 8 and Figure 10, respectively. As is evidenced from Figure 8, the states close to Fermi level (E_F) are dominated by Ir d -states strongly hybridized with O p -states. The dominating part of O p -states separated from Fe and Ir d -states are located below Fermi level within the range from -7.8 eV to -2.4 eV. In the majority spin channel, the Fe t_{2g} , as well as e_g states, remain filled while in Ir-sites the t_{2g} states are completely filled and the e_g states remain empty. In the minority spin channel, the Fe t_{2g} and e_g states remain completely empty while in Ir-sites the t_{2g} states remain filled and the e_g states stay completely empty, thus give rise to an insulating character in both the spin channels. This rare FM insulating nature of BFIO makes it very special.

Figure. 10 depicts the DOS of FiM metallic phase when the on-site Coulomb repulsion is switched off on 5d (Ir)-sites. The metallic character of this state comes from the Ir majority spin channel due to the presence of a hole in t_{2g} states (see also Figure 9). However, in the minority spin channel, all the t_{2g} states of Ir are occupied. It is noticed that the t_{2g} states of Fe and Ir co-exist around the Fermi level with a finite hybridization between them. In this state, Ir ion is in formal oxidation state 4+ and Fe takes high spin 2+ state, at $U = 6.38$ (Fe), 0 (Ir) (see Figure 7). Due to these electronic configurations of outer valence shells and nearly 149° Fe-O-Ir angle, the magnetic moments of Fe and Ir interacts through an antiferromagnetic superexchange mechanism satisfying the Goodenough-Kanamori (GK) rules [37–39]. Therefore, the system ends up with a FiM configuration with a total mag-

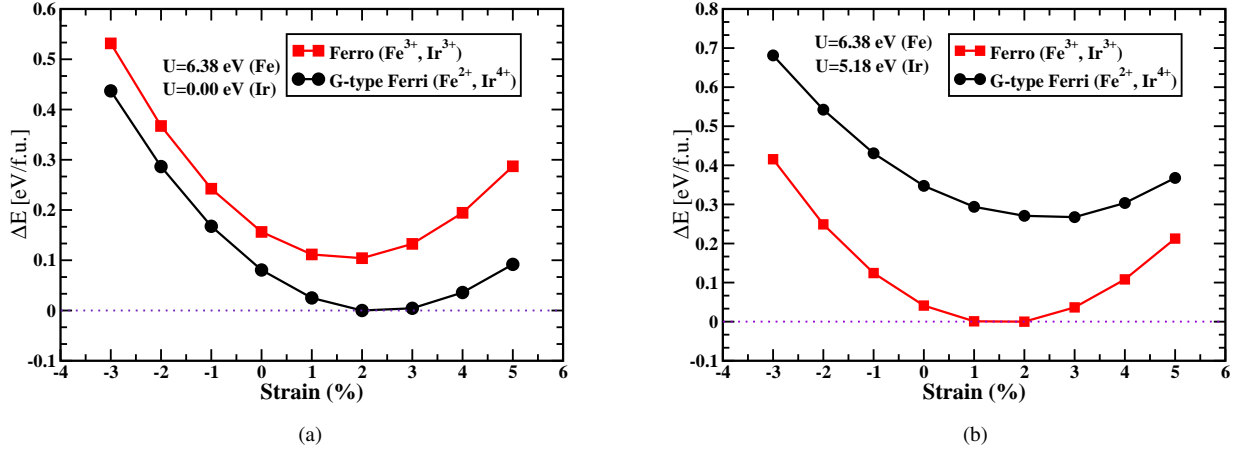


FIG. 6. (a) Strain dependence structural stability of $\text{Bi}_2\text{FeIrO}_6$ thin films. Optimized energies are positioned as a function of biaxial with respect to the G-type ferrimagnetic structure at +2% strain. All the energies were optimized using GGA+ U (Fe) approach. The solid black line denotes the ferrimagnetic metallic structure and the solid red line represents the ferromagnetic insulator. (b) Illustrates the energy vs biaxial strain where the energies are positioned with respect to the ferromagnetic structure at +2% strain. The energies were obtained using the GGA+ U method with $U_{eff} = 6.38, 5.18$ eV for Fe and Ir, respectively. Like Figure 6(a), the solid black line denotes the ferrimagnetic metallic state and that of the solid red line denotes the ferromagnetic insulator, as the lowest energy state.

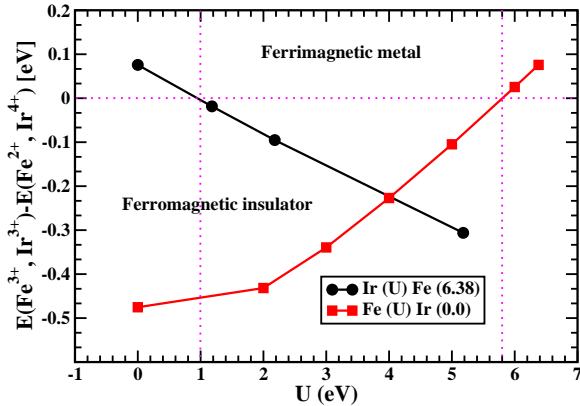


FIG. 7. Phase diagram of monoclinic $P2_1/n$ structure on energy (E)-correlation (U) plane. There are two phases, the plane just above the dotted horizontal line is ferrimagnet metallic and one just below it is a ferromagnetic insulator. The solid black line represents the change in energy by varying U on Ir-sites keeping the U on Fe-site fixed. Similarly, the red line shows the change in energy by varying U on Fe-sites fixing $U = 0$ on Ir-sites.

netic moment of $1 \mu_B/\text{f.u.}$ Like the FM insulating state, the metallic AFM states are also very special due to their rare existence.

As we know, $5d$ transition metals have an intrinsically strong spin-orbit coupling (SOC). Particularly, iridates are known to display SOC effect [40–45] in perovskites and DPs. Motivated by this, we extended our calculation to consider the SOC effect on top of GGA as well as GGA+ U functionals. We observed that adding SOC to GGA, lowered the band gap, while the insulating behavior was recovered by adding

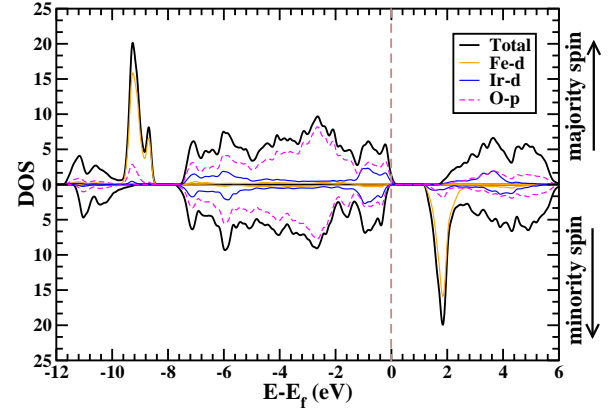


FIG. 8. The density of states (DOS) of FM $\text{Bi}_2\text{FeIrO}_6$, calculated using the GGA+ U method with $U_{eff} = 6.38, 5.18$ eV for Fe and Ir, respectively. The dashed vertical zero line is set to the Fermi energy. The local magnetic moments on Ir site are antialigned with equal magnitude leading to zero magnetic moment, while on Fe site the up spin channel is completely filled and the down spin channel is completely empty, hence results in a net magnetic moment in the system. The solid black line, total DOS; orange solid line, Fe- d states; blue line, Ir- d states and solid magenta line, O- p states.

U . However, there is no major change in the magnetic properties of the system. Once again the system preferred to stay in the $\text{Fe}^{3+}, \text{Ir}^{3+}$ oxidation state even with SOC. The low spin $3+$ oxidation state of Ir (d^6) ion, weakens the role of SOC in BFIO.

As can be seen in Fig. 8, the conduction band is made up almost entirely by Fe states whereas valence band results from Ir-O hybridised states. In principle, this implies that the photoexcitation can lead to electron-hole separation in the sublattices.

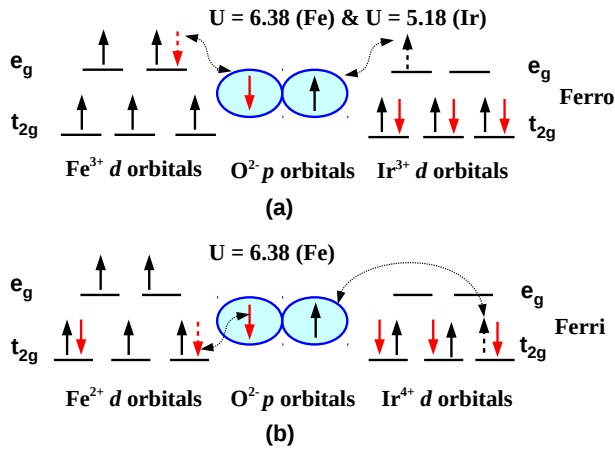


FIG. 9. Schematic level diagrams of $3d$ - $5d$ orbitals. (a) Schematic representation of the $3d$ - $5d$ electrons of d orbitals in Fe^{3+} , Ir^{3+} oxidation state. The interaction between the two transition metals via O p orbitals leads to ferromagnetism. (b) Representation of the $3d$ - $5d$ electrons of d orbitals in Fe^{2+} , Ir^{4+} oxidation state. For case (b) the interaction between the atom leads to an AFM. The antiferromagnetic and ferromagnetic interaction basically depends on the occupations of the e_g orbitals.

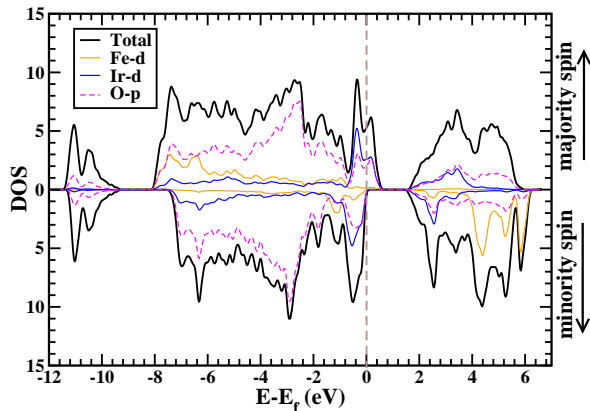


FIG. 10. The density of states (DOS) of G-type AFM Bi_2FeIrO_6 , calculated using GGA+ U method with $U_{eff}=6.38$, 0.0 eV for Fe and Ir, respectively. The dashed vertical zero line is set to the Fermi energy. The local magnetic moments on Fe and Ir are antialigned with unequal magnitude leading to a net magnetic moment on the system. The solid black line, total DOS; green solid line, Fe- d states; blue line, Ir- d states and solid magenta line, O - p states.

tices which is a desirable feature for photovoltaic applications.

SUMMARY

In summary, we have designed two Bi-based double-perovskites Bi_2FeReO_6 and Bi_2FeIrO_6 mimicking the thin-film geometry grown along [001] direction. These two structures were constructed by keeping the Fe atom fixed at B-site and substituting Re and Ir ($5d$) atoms in B'-sites of ordered DP

$A_2BB'O_6$ structure. The calculated tolerance factors indicate that both the compounds will adopt perovskite (orthorhombic/monoclinic) crystal structure. The Bi_2FeReO_6 thin-film becomes stable adopting a monoclinic $P2_1/n$ phase under a wide range of ES. By incorporating various types of magnetic ordering we show that the thin-film Bi_2FeReO_6 prefers a C-AFM spin ordering in its ground-state with zero magnetic moments. However, at -2.7% strain the structure adopts G-AFM ordering through a monoclinic to monoclinic structural transition. The G-AFM phase of BFRO provides a magnetic moment of $1 \mu_B/f.u.$ which is comparable to the previously reported Bi-based $3d$ - $5d$ compounds [24]. Our DOS calculations indicate that the Bi_2FeReO_6 is an insulator with a band gap of around 1.2 eV in thin film form. We find the correlation effect on Re ($5d$)-site to be very important, as on-site Coulomb repulsion (U) widens the band gap significantly. In this compound, Fe takes a high spin 2+ oxidation state, whereas Re adopts its formal high spin 4+ state. One important finding of our calculations is that the oxygen octahedra around Fe atoms undergo a distortion leading to long-short Fe-O bonds in the octahedra, which is not observed in the BFIO thin-film.

In Bi_2FeIrO_6 the $P2_1/n$ symmetry structure emerged as the ground state. Both the transition metals (Fe, Ir) takes 3+ oxidation state, where Fe acquires high spin configuration and Ir prefers to stay in a low spin. This configuration of Bi_2FeIrO_6 leads to a huge ferromagnetic ground state with a magnetic moment of $5 \mu_B/f.u.$ throughout the considered ES. However, when the onsite Coulomb repulsion term on Ir-site is switched off, the system stabilizes in FiM ground state with a magnetic moment of $3 \mu_B/f.u.$ over the ES. The DOS calculations show that the FM state is an insulator while the FiM state is a half-metal. Our calculations show that even a small value of U on Ir site could, in principle, switch the (2+, 4+) oxidation state to (3+, 3+) state. So, there is a correlation driven metal to insulator transition in BFIO thin-film under ES. Given that ferromagnetic insulators and antiferromagnetic metals are very rare, the *ab initio* designed BFIO could prove to be quite technologically significant.

Both the compounds can be used in spintronic applications due to their magnetic and half-metallic nature. Apart from this, their narrow band-gaps (~ 1.2 and 1.3 , respectively) make them a suitable candidate for PV applications. Although these materials are not ferroelectric, an appropriate doping strategy can make them ferroelectric [19, 46]. Apart from PV applications, these materials can also be used for the photocatalytic activity, such as solar water splitting and water purification. Like the parent BFO compound, the narrow band gap nature of these $3d$ - $5d$ compounds could allow them to harvest parts of the visible light of the solar spectrum. We hope that our observations will initiate further experimental efforts to verify the interesting predictions made in this work.

The authors would like to thank Dr. D. S. Rana at IISER Bhopal for helpful discussions. The authors gratefully acknowledge IISER Bhopal for computational resources and funding. PCR is thankful to Council of Scientific and Industrial Research, India, for the research fellowship.

-
- [1] M. M. Vopson, *Crit. Rev. Solid State Mater. Sci.* **40**, 223 (2015).
- [2] N. A. Spaldin and M. Fiebig, *Science* **309**, 391 (2005).
- [3] G. Catalan and J. F. Scott, *Adv. Mater.* **21**, 2463 (2009).
- [4] P. Baettig and N. A. Spaldin, *Appl. Phys. Lett.* **86**, 012505 (2005).
- [5] D. Meng, H. Guo, Z. Cui, C. Ma, J. Zhao, J. Lu, H. Xu, Z. Wang, X. Hu, Z. Fu, *et al.*, *Proc. Natl. Acad. Sci. U.S.A.* **115**, 2873 (2018).
- [6] X.-Z. Lu and J. M. Rondinelli, *Nat. Mater.* **15**, 951 (2016).
- [7] J. H. Lee and K. M. Rabe, *Phys. Rev. Lett.* **104**, 207204 (2010).
- [8] H. Chen and A. J. Millis, *Phys. Rev. B* **94**, 165106 (2016).
- [9] Q. Gan, R. Rao, C. Eom, J. Garrett, and M. Lee, *Appl. Phys. Lett.* **72**, 978 (1998).
- [10] I. Grinberg, D. V. West, M. Torres, G. Gou, D. M. Stein, L. Wu, G. Chen, E. M. Gallo, A. R. Akbashev, P. K. Davies, *et al.*, *Nature* **503**, 509 (2013).
- [11] T. Choi, S. Lee, Y. Choi, V. Kiryukhin, and S.-W. Cheong, *Science* **324**, 63 (2009).
- [12] R. Nechache, C. Harnagea, S. Licoccia, E. Traversa, A. Ruediger, A. Pignolet, and F. Rosei, *Appl. Phys. Lett.* **98**, 202902 (2011).
- [13] R. Nechache, C. Harnagea, S. Li, L. Cardenas, W. Huang, J. Chakrabarty, and F. Rosei, *Nat. Photonics* **9**, 61 (2015).
- [14] D. Kim, H. Han, J. H. Lee, J. W. Choi, J. C. Grossman, H. M. Jang, and D. Kim, *Proc. Natl. Acad. Sci. U.S.A.*, 201721503 (2018).
- [15] P. C. Rout, A. Putatunda, and V. Srinivasan, *Phys. Rev. B* **93**, 104415 (2016).
- [16] A. Khare, A. Singh, S. S. Prabhu, and D. S. Rana, *Appl. Phys. Lett.* **102**, 192911 (2013).
- [17] S. et al., *J. Appl. Phys.* **116**, 114901 (2014).
- [18] G. V. et al., *APL Mater.* **3**, 116107 (2015).
- [19] P. C. Rout and V. Srinivasan, arXiv preprint arXiv:1807.01649 (2018).
- [20] M. Ležaić and N. A. Spaldin, *Phys. Rev. B* **83**, 024410 (2011).
- [21] H. L. Feng, M. Arai, Y. Matsushita, Y. Tsujimoto, Y. Guo, C. I. Sathish, X. Wang, Y.-H. Yuan, M. Tanaka, and K. Yamaura, *J. Am. Chem. Soc.* **136**, 3326 (2014).
- [22] Y. Krockenberger, K. Mogare, M. Reehuis, M. Tovar, M. Jansen, G. Vaitheeswaran, V. Kanchana, F. Bultmark, A. Delin, F. Wilhelm, A. Rogalev, A. Winkler, and L. Alff, *Phys. Rev. B* **75**, 020404 (2007).
- [23] L. Wang, Y. Li, A. Bera, C. Ma, F. Jin, K. Yuan, W. Yin, A. David, W. Chen, W. Wu, W. Prellier, S. Wei, and T. Wu, *Phys. Rev. Applied* **3**, 064015 (2015).
- [24] M. Ležaić and N. A. Spaldin, *Phys. Rev. B* **83**, 024410 (2011).
- [25] V. I. Anisimov, F. Aryasetiawan, and A. I. Liechtenstein, *J. Phys. Condens. Matter* **9**, 767 (1997).
- [26] M. Cococcioni and S. de Gironcoli, *Phys. Rev. B* **71**, 035105 (2005).
- [27] B. Himmetoglu, R. M. Wentzcovitch, and M. Cococcioni, *Phys. Rev. B* **84**, 115108 (2011).
- [28] J. P. Perdew, K. Burke, and M. Ernzerhof, *Phys. Rev. Lett.* **77**, 3865 (1996).
- [29] J. P. Perdew, K. Burke, and M. Ernzerhof, *Phys. Rev. Lett.* **78**, 1396 (1997).
- [30] J. P. Perdew, A. Ruzsinszky, G. I. Csonka, O. A. Vydrov, G. E. Scuseria, L. A. Constantin, X. Zhou, and K. Burke, *Phys. Rev. Lett.* **100**, 136406 (2008).
- [31] P. Giannozzi et al, *J. Phys. Condens. Mater.* **21**, 395502 (2006).
- [32] A. Glazer, *Acta Crystallographica Section A: Crystal Physics, Diffraction, Theoretical and General Crystallography* **31**, 756 (1975).
- [33] A. Glazer, *Acta Crystallographica Section B: Structural Crystallography and Crystal Chemistry* **28**, 3384 (1972).
- [34] A. Janotti, B. Jalan, S. Stemmer, and C. G. V. de Walle, *Appl. Phys. Lett.* **100**, 262104 (2012).
- [35] H. P. S. Corrêa, I. P. Cavalcante, D. O. Souza, E. Z. Santos, M. T. D. Orlando, H. Belich, F. J. Silva, E. F. Medeiro, J. M. Pires, J. L. Passamai, L. G. Martinez, and J. L. Rossi, *Cerâmica* **56**, 193 (2010).
- [36] D. Serrate, J. M. D. Teresa, and M. R. Ibarra, *J. Phys.: Condens. Matter* **19**, 023201 (2007).
- [37] J. B. Goodenough, *Phys. Rev.* **100**, 564 (1955).
- [38] J. Kanamori, *J. Phys. Chem. Solids* **10**, 87 (1959).
- [39] E. O. Wollan, *Phys. Rev.* **117**, 387 (1960).
- [40] X. Ou and H. Wu, *Sci. Rep.* **4**, 4609 (2014).
- [41] J. G. Zhao, L. X. Yang, Y. Yu, F. Y. Li, R. C. Yu, Z. Fang, L. C. Chen, and C. Q. Jin, *J. Appl. Phys.* **103**, 103706 (2008).
- [42] M. A. Zeb and H.-Y. Kee, *Phys. Rev. B* **86**, 085149 (2012).
- [43] Y. F. Nie, P. D. C. King, C. H. Kim, M. Uchida, H. I. Wei, B. D. Faeth, J. P. Ruf, J. P. C. Ruff, L. Xie, X. Pan, C. J. Fennie, D. G. Schlom, and K. M. Shen, *Phys. Rev. Lett.* **114**, 016401 (2015).
- [44] K.-H. Kim, H.-S. Kim, and M. J. Han, *J. Phys.: Condens. Matter* **26**, 185501 (2014).
- [45] D. Haskel, G. Fabbris, M. Zhernenkov, P. P. Kong, C. Q. Jin, G. Cao, and M. van Veenendaal, *Phys. Rev. Lett.* **109**, 027204 (2012).
- [46] H. J. Zhao, W. Ren, Y. Yang, J. Íñiguez, X. M. Chen, and L. Bellaiche, *Nature communications* **5**, 4021 (2014).